Biophysical Journal
P. 259–267 (1994)
Please send to
Peter Bassen

MR Diffusion *Tensor* Spectroscopy and Imaging

Peter J. Basser,* James Mattiello,* and Denis LeBihan‡

*Biomedical Engineering and Instrumentation Program, National Center for Research Resources, and ‡Diagnostic Radiology Department, The Warren G. Magnuson Clinical Center, National Institutes of Health, Bethesda, Maryland 20892 USA

ABSTRACT This paper describes a new NMR imaging modality—MR diffusion *tensor* imaging. It consists of estimating an effective diffusion tensor, $\mathbf{D}_{\text{eff}}$, within a voxel, and then displaying useful quantities derived from it. We show how the phenomenon of anisotropic diffusion of water (or metabolites) in anisotropic tissues, measured noninvasively by these NMR methods, is exploited to determine fiber tract orientation and mean particle displacements. Once $\mathbf{D}_{\text{eff}}$ is estimated from a series of NMR pulsed-gradient, spin-echo experiments, a tissue's three orthotropic axes can be determined. They coincide with the eigenvectors of $\mathbf{D}_{\text{eff}}$, while the effective diffusivities along these orthotropic directions are the eigenvalues of $\mathbf{D}_{\text{eff}}$. Diffusion ellipsoids, constructed in each voxel from $\mathbf{D}_{\text{eff}}$, depict both these orthotropic axes and the mean diffusion distances in these directions. Moreover, the three scalar invariants of $\mathbf{D}_{\text{eff}}$, which are independent of the tissue's orientation in the laboratory frame of reference, reveal useful information about molecular mobility reflective of local microstructure and anatomy. Inherently, tensors (like $\mathbf{D}_{\text{eff}}$) describing transport processes in anisotropic media contain new information *within a macroscopic voxel* that scalars (such as the apparent diffusivity, proton density, T_1, and T_2) do not.

INTRODUCTION

NMR imaging has been used to measure the diffusivity of water and metabolites noninvasively in vivo at microscopic length scales (LeBihan and Breton, 1985). In tissues such as brain white matter (Chenevert et al., 1990; Doran et al., 1990; Douek et al., 1991; LeBihan, 1991; LeBihan et al., 1993; Moseley et al., 1990), skeletal muscle (Cleveland et al., 1976), and bovine tendon (Fullerton et al., 1985), the apparent (scalar) diffusivity of water depends on the angle between the fiber-tract axis and the applied magnetic field gradient. Specifically, the apparent diffusivity is largest when this diffusion-sensitizing gradient is parallel to the fiber direction and smallest when it is perpendicular to it (Chenevert et al., 1990; Cleveland et al., 1976; Douek et al., 1991; LeBihan et al., 1993; Moseley et al., 1990). The most plausible explanation for this phenomenon is that cell membranes and other oriented molecular structures retard diffusion of water perpendicular to the fiber tract axis more than parallel to it. While both Moseley (Moseley et al., 1990) and Douek (Douek et al., 1991) suggested that anisotropic diffusion could be used to determine nerve fiber tract orientation within brain white matter, we propose a general and objective method to determine the orientation of the fiber tracts in tissues noninvasively in vivo, using anisotropic diffusion.

However, the dependence of the apparent (scalar) diffusivity on the applied magnetic field gradient direction is only indicative of diffusion anisotropy. In tissues, such as brain white matter and skeletal muscle, an effective diffusion tensor, $\mathbf{D}_{\text{eff}}$, should be used to characterize it. Diffusion in these tissues is heterogeneous at a microscopic (cellular) length scale (i.e., the diffusivity depends upon position) but is homogeneous and anisotropic at a macroscopic (voxel) length scale. In such anisotropic media, the macroscopic diffusive flux vector, $\mathbf{J}$, is not necessarily parallel to the macroscopic concentration gradient vector, ∇C, as it is in isotropic media, and Fick's first law (written in vector form) is written as $\mathbf{J} = -\mathbf{D}_{\text{eff}} \nabla C$. Both microscopic and macroscopic continuum viewpoints are illustrated in Fig. 1.

Previously, we showed how to estimate $\mathbf{D}_{\text{eff}}$ (both its diagonal and off-diagonal elements) from a series of pulsed-gradient, spin-echo NMR experiments (Basser and LeBihan, 1992; Basser et al., 1992, 1994) using multivariate linear regression. Here, we show how to use this estimated $\mathbf{D}_{\text{eff}}$ to elucidate the fiber-tract directions within an anisotropic medium. More generally, we determine its three orthotropic directions, the effective diffusion coefficients, and the mean molecular displacements along them. Moreover, we also identify three scalar quantities that are independent of fiber direction, depending only on the composition and local microstructure of the tissue. Finally, we generalize the estimation of a single effective diffusion tensor for a sample (diffusion tensor MR spectroscopy) to the estimation of an effective diffusion tensor in each voxel (diffusion tensor MR imaging) from a sequence of diffusion-weighted MR images.

PRINCIPLES

Relating the spin-echo intensity and D_{eff}

Bloch's equations of magnetic induction (Bloch, 1946) were recast as a magnetization transport equation that describes both isotropic (Torrey, 1956) and anisotropic diffusion (Stejskal, 1965; Stejskal and Tanner, 1965). In particular, for a 90°–180° spin-echo, pulsed-gradient experiment, analytic expressions have been derived that relate the measured echo intensity to the applied pulse gradient sequence (Stejskal and Tanner, 1965). For isotropic media, the magnitude of the

Received for publication 24 March 1993 and in final form 7 October 1993.

Address reprint requests to Dr. Peter J. Basser, Building 13, Room 3W13, 9000 Rockville Pike, BEIP, NCRR, NIH, Bethesda, MD 20892.

0006-3495/94/01/259/09 $2.00

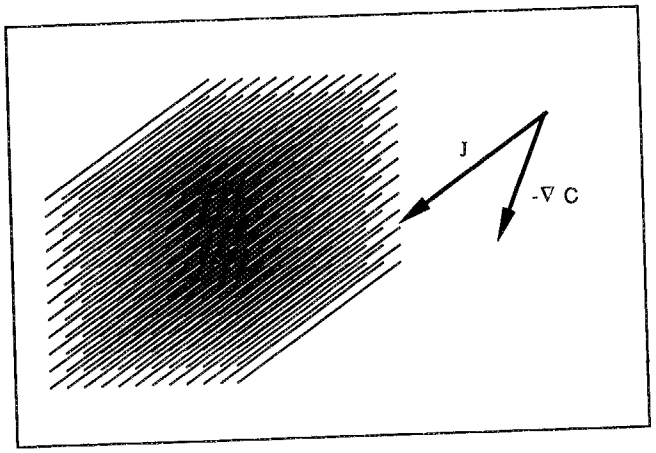

FIGURE 1 A schematic diagram of an array of microscopic fiber bundles (e.g., bundles of myelinated axons) viewed at a macroscopic (voxel) length scale. At the macroscopic length scale, particle flux and concentration gradient vectors are not necessarily parallel.

magnetization at the time of the echo, $A(TE)$, is related to the scalar self-diffusivity, D, by

$$\ln\left[\frac{A(TE)}{A(0)}\right] = -\gamma^2 \int_0^{TE} \left(\mathbf{F}(t') - 2H\left(t' - \frac{TE}{2}\right)\mathbf{f}\right)^T \cdot D\left(\mathbf{F}(t') - 2H\left(t' - \frac{TE}{2}\right)\mathbf{f}\right) dt'. \quad (1)$$

Above, γ is the gyromagnetic ratio of protons, $A(0)$ is the initial transverse magnetization (at $t = 0^+$) just after the 90° pulse is applied, and $H(t)$ is the unit Heaviside function. In addition,

$$\mathbf{G}(t) = (G_x(t), G_y(t), G_z(t))^T \quad (2)$$

is the applied magnetic field gradient (column) vector, and

$$\mathbf{G}(t) = \int_0^t \mathbf{F}(t'')\, dt''; \quad \mathbf{f} = \mathbf{F}\left(\frac{TE}{2}\right). \quad (3)$$

From Eq. 1, Tanner defined an effective scalar diffusion coefficient, D_{eff}, that is averaged over the echo time, TE (Tanner, 1978). The relationship between the effective diffusivity and the logarithm of the echo intensity can be written as

$$\ln\left[\frac{A(TE)}{A(0)}\right] = -bD_{\text{eff}}, \quad (4)$$

where

$$b = \gamma^2 \int_0^{TE} \left(\mathbf{F}(t') - 2H\left(t' - \frac{TE}{2}\right)\mathbf{f}\right)^T \left(\mathbf{F}(t') - 2H\left(t' - \frac{TE}{2}\right)\mathbf{f}\right) dt'. \quad (5)$$

Moreover, for anisotropic media, Stejskal and Tanner related $A(TE)$ to the diffusion tensor, $\mathbf{D}$ (Stejskal and Tanner, 1965):

$$\ln\left[\frac{A(TE)}{A(0)}\right] = -\gamma^2 \int_0^{TE} \left(\mathbf{F}(t') - 2H\left(t' - \frac{TE}{2}\right)\mathbf{f}\right)^T \mathbf{D}\left(\mathbf{F}(t') - 2H\left(t' - \frac{TE}{2}\right)\mathbf{f}\right) dt'. \quad (6)$$

By analogy, we recently defined an *effective* diffusion tensor, $\mathbf{D}_{\text{eff}}$, that is also averaged over the echo time, TE (Basser et al., 1992, 1994). We showed previously that Eq. 6 could be rewritten as a linear relationship between the logarithm of the echo intensity and each component of $\mathbf{D}_{\text{eff}}$ (Basser et al., 1992, 1994):

$$\ln\left[\frac{A(TE)}{A(0)}\right] = -\sum_{i=1}^{3}\sum_{j=1}^{3} b_{ij} D_{\text{eff}\,ij}, \quad (7)$$

where b_{ij} are elements of the b matrix, $\mathbf{b}$ (Basser et al., 1992, 1994), defined as

$$\mathbf{b} = \gamma^2 \int_0^{TE} \left(\mathbf{F}(t') - 2H\left(t' - \frac{TE}{2}\right)\mathbf{f}\right) \left(\mathbf{F}(t') - 2H\left(t' - \frac{TE}{2}\right)\mathbf{f}\right)^T dt'. \quad (8)$$

The b matrix in Eq. 8 can be calculated off-line from the prescribed magnetic field gradient pulse sequences, Eqs. 2 and 3, either numerically or analytically (Mattiello et al., 1994). It accounts for "cross-terms" (Neeman et al., 1990) that arise not only from well-known interactions between imaging and diffusion gradients applied in the same direction (which are included in the diagonal elements of b_{ij}), but also from interactions between imaging and diffusion gradients applied in *perpendicular* directions (which are included in the off-diagonal elements of b_{ij}). Interactions between these orthogonal gradients have not been discussed previously in the context of NMR diffusion spectroscopy and imaging applications. Ignoring their effect in diffusion tensor spectroscopy (Basser et al., 1994) and imaging (Mattiello et al., 1993) can corrupt the estimate of the effective diffusion tensor.

Just as Tanner (1978) used Eq. 4 to estimate $\mathbf{D}_{\text{eff}}$ in microscopically heterogeneous but macroscopically isotropic media using univariate linear regression, we use Eq. 7 to estimate $\mathbf{D}_{\text{eff}}$ in microscopically heterogeneous but macroscopically anisotropic media using weighted multivariate linear regression. Moreover, just as LeBihan and others have used Eqs. 4 and 5 to estimate $\mathbf{D}_{\text{eff}}$ within a voxel, which is called MR diffusion imaging (LeBihan and Breton, 1985; LeBihan et al., 1986; Merboldt et al., 1985), we use Eqs. 2, 3, 7, and 8 to estimate $\mathbf{D}_{\text{eff}}$ in a voxel, which we call MR diffusion *tensor* imaging.

Principal coordinate axes and principal diffusivities

For each estimated $\mathbf{D}_{\text{eff}}$, whether it is measured for an entire tissue sample or for an individual voxel, we can construct a local orthogonal coordinate system (the principal coordinate axes) along which diffusive fluxes and concentration gradients are decoupled. Moreover, we can calculate three corresponding diffusion coefficients in these three principal directions (principal diffusivities). Because $\mathbf{D}_{\text{eff}}$ is symmetric and positive definite, its three eigenvectors (principal coordinate directions) ϵ_1, ϵ_2, and ϵ_3 are orthogonal. Related to them are three positive eigenvalues (principal effective diffusivities), λ_1, λ_2, and λ_3:

$$\mathbf{D}_{\text{eff}}\boldsymbol{\epsilon}_i = \lambda_i \boldsymbol{\epsilon}_i \quad \text{for} \quad i = \{1, 2, 3\}. \tag{9}$$

The three equations in Eq. 9 can be rewritten in matrix form as

$$\mathbf{D}_{\text{eff}}\mathbf{E} = \mathbf{E}\boldsymbol{\Lambda} \qquad \text{with} \quad \mathbf{E} = (\boldsymbol{\epsilon}_1 \mid \boldsymbol{\epsilon}_2 \mid \boldsymbol{\epsilon}_3)$$
$$\text{and} \quad \boldsymbol{\Lambda} = \begin{pmatrix} \lambda_1 & 0 & 0 \\ 0 & \lambda_2 & 0 \\ 0 & 0 & \lambda_3 \end{pmatrix}, \tag{10}$$

where $\boldsymbol{\Lambda}$ is the diagonal matrix of eigenvalues and $\mathbf{E}$ is the matrix of orthonormal eigenvectors, arranged in columns.

As suggested above, in ordered structures such as brain white matter and skeletal muscle, the macroscopic anisotropy described by $\mathbf{D}_{\text{eff}}$ at a macroscopic voxel length scale is due to microscopic heterogeneity—primarily to ordered, semipermeable membranes that retard diffusion (Douek et al., 1991). So, in anisotropic fibrous tissues, the principal directions of $\mathbf{D}_{\text{eff}}$ must coincide with the orthotropic directions of that tissue. In particular, the eigenvector associated with the largest eigenvalue (diffusivity) defines the tissue's fiber-tract axis, while the two remaining eigenvectors perpendicular to it should define the two remaining orthotropic axes.

Effective diffusion ellipsoid

For anisotropic media, the effective diffusion tensor, $\mathbf{D}_{\text{eff}}$, inherently contains more information than a scalar apparent diffusivity, some of which can be represented graphically by an effective diffusion ellipsoid. To motivate its use and interpret its meaning, it is helpful to represent molecular diffusion in an anisotropic medium as a Brownian random process characterized by a macroscopic Gaussian conditional probability density function, $\rho(\mathbf{x} \mid \mathbf{x}_0, t)$ (Stejskal, 1965)—the probability that the spin-labeled species initially at $\mathbf{x}_0$ and $t = 0$ reaches position $\mathbf{x}$ at time t:

$$\rho(\mathbf{x} \mid \mathbf{x}_0, \tau) = \frac{1}{\sqrt{|\mathbf{D}_{\text{eff}}(\tau)|\,(4\pi\tau)^3}} \exp\left[\frac{-(\mathbf{x} - \mathbf{x}_0)^T \mathbf{D}_{\text{eff}}^{-1}(\tau)(\mathbf{x} - \mathbf{x}_0)}{4\tau}\right]. \tag{11}$$

Above, $\mathbf{D}_{\text{eff}}^{-1}(\tau)$, which is assumed to be uniform within a voxel, can be interpreted as a covariance matrix of this translational displacement distribution, $\rho(\mathbf{x} \mid \mathbf{x}_0, \tau)$. It is written as an explicit function of time, because it may vary with the diffusion time or with the duration of the experiment. In tissue, we would expect $\mathbf{D}_{\text{eff}}^{-1}(\tau)$ to be isotropic for very short diffusion times, until a significant number of protons encounter permeable barriers (Tanner, 1978). For longer diffusion times, we would expect the ellipsoids to become more prolate. However, for media with impermeable barriers, the Gaussian displacement distribution assumed above may not adequately represent the observed displacement distribution (Cory, 1990).

We can construct an effective diffusion ellipsoid by setting the quadratic form in the exponent of $\rho(\mathbf{x} \mid \mathbf{x}_0, \tau)$ in Eq. 11 to ½, i.e.,

$$\frac{(\mathbf{x} - \mathbf{x}_0)^T \mathbf{D}_{\text{eff}}^{-1}(\tau)(\mathbf{x} - \mathbf{x}_0)}{2\tau} = 1 \tag{12}$$

The shape of the effective diffusion ellipsoid has a useful physical interpretation. If we imagine that the tissue were *microscopically* homogeneous and anisotropic, with a diffusion tensor $\mathbf{D} = \mathbf{D}_{\text{eff}}(\tau)$, then Eq. 12 defines a surface of constant mean translational displacement of spin-labeled particles at time $t = \tau$. To make this explicit, we first transform[1] coordinates from the "laboratory" frame ($\mathbf{x}$) in which the components of $\mathbf{D}_{\text{eff}}(\tau)$ are measured to the "principal" or "fiber" frame ($\mathbf{x}'$) of reference within a particular voxel centered at $\mathbf{x}_0$, using

$$\mathbf{x}' = \mathbf{E}^T(\mathbf{x} - \mathbf{x}_0). \tag{13}$$

Then, using Eqs. 13 and 10, the quadratic form in Eq. 12 becomes

$$\frac{\mathbf{x}'^T \boldsymbol{\Lambda}^{-1} \mathbf{x}'}{2\tau} = 1. \tag{14}$$

When expanded, Eq. 14 becomes

$$\left(\frac{x'}{\sqrt{2\lambda_1\tau}}\right)^2 + \left(\frac{y'}{\sqrt{2\lambda_2\tau}}\right)^2 + \left(\frac{z'}{\sqrt{2\lambda_3\tau}}\right)^2 = 1. \tag{15}$$

In the "fiber" frame, where the displacement distribution becomes uncorrelated, the material's local orthotropic directions coincide with the principal axes of the ellipsoid. The ellipsoid's major axes, from Eq. 15, are the mean effective diffusion distances ($\sqrt{\langle x_i'^2 \rangle} = \sqrt{2\lambda_i\tau}$) in the three principal (orthotropic) directions at time τ. Therefore, the effective diffusion ellipsoid depicts both the fiber-tract direction and the mean diffusion distances.

Scalar invariants of $\mathbf{D}_{\text{eff}}$

Identification of quantities that are independent of fiber direction is as important as identifying fiber direction itself.

[1] We should ensure that $\mathbf{E}$ has the properties of coordinate transformation, e.g., $\det(\mathbf{E}) = 1, \cdots$.

Three examples are the scalar invariants, I_1, I_2, and I_3 (Fung, 1977) associated with $\mathbf{D}_{\text{eff}}$ in each voxel. They are functions only of the eigenvalues (principal diffusivities) of $\mathbf{D}_{\text{eff}}$:

$$I_1 = \lambda_1 + \lambda_2 + \lambda_3 = \text{Tr}(\mathbf{D}_{\text{eff}}) = \text{Tr}(\mathbf{\Lambda}) \quad (16a)$$

$$I_2 = \lambda_1\lambda_2 + \lambda_3\lambda_1 + \lambda_2\lambda_3 \quad (16b)$$

$$I_3 = \lambda_1\lambda_2\lambda_3 = |\mathbf{D}_{\text{eff}}| = |\mathbf{\Lambda}| \quad (16c)$$

These scalar quantities I_1, I_2, and I_3 are invariant with respect to rotation of the coordinate system, and consequently are independent of the laboratory reference frame in which $\mathbf{D}_{\text{eff}}$ is measured (i.e., they have the same value irrespective of the relative orientation of the "laboratory" and "fiber" frames of reference). Moreover, they are insensitive to the scheme by which the eigenvalues of $\mathbf{D}_{\text{eff}}$ are ordered (numbered). As such, these invariants measure intrinsic properties of the medium, and are expected to be useful in characterizing the local microstructure and anatomy of anisotropic tissue. Moreover, they (or functions of them) are easily measured and monitored.

By normalizing each scalar invariant by the self-diffusivity of water, D_w (at the known temperature of the sample), raised to the appropriate power[2] we can compare each invariant to its value in free solution.

Other dimensionless ratios of the eigenvalues can be used to measure the degree of diffusion anisotropy. For example, one dimensionless anisotropy ratio, λ_2/λ_3, measures the degree of rotational symmetry around the longest (fiber) axis (with $\lambda_2/\lambda_3 = 1$ indicating rotational symmetry), while λ_1/λ_2 and λ_1/λ_3 measure the relative magnitude of the diffusivities in the fiber and transverse directions. These anisotropy ratios are also insensitive to the sample's orientation with respect to the (laboratory) x-y-z reference frame. They measure the ratio of the effective diffusivities both parallel to and perpendicular to the fiber tract directions, independent of the sample's placement and orientation within the magnet. An anisotropy ratio proposed by Douek et al. (Douek et al., 1991), defined as the quotient of two diagonal elements of the diffusion tensor (e.g., D_{xx}/D_{zz}), would vary as the sample is rotated (Basser et al., 1992). This definition is at odds with our intuitive notion that an anisotropy ratio is a characteristic of the tissue and, as such, is independent of the sample's placement or orientation. Only when the sample's orthotropic axes are coincident with the laboratory frame of reference will the anisotropy ratios proposed by Douek et al. (Douek et al., 1991) equal the ratio of the effective diffusion coefficients parallel to and perpendicular to the fiber tracts, an unlikely condition for most NMR imaging applications.

MATERIALS AND METHODS

Diffusion tensor NMR spectroscopy was previously performed with water and pork-loin samples, using a surface coil in a 4.7-Tesla Spectrometer-Imager (GE Omega™, Fremont, CA) (Basser and LeBihan, 1992; Basser et al., 1994). These methods are repeated here because they are required to explain the diffusion tensor imaging protocol described in the following paragraph. Pulsed-gradient, spin-echo sequences, incorporating symmetric trapezoidal gradient pulses, as shown in Fig. 2, were applied sequentially in seven noncollinear directions: $\mathbf{G}^T = (G_x, G_y, G_z)^T = G_0$ {(1, 0, 0), (0, 1, 0), (0, 0, 1), (1, 0, 1), (1, 1, 0), (0, 1, 1), and (1, 1, 1)} (Basser and LeBihan, 1992; Basser et al., 1992, 1994). In each of the seven directions, the gradient strength, G_0, was increased (in 1-G/cm increments) from 1 to 14 or 15 G/cm three times, so that the total number of single acquisitions, N, was either 294 or 315 (Basser and LeBihan, 1992; Basser et al., 1994). For each spectroscopic spin-echo experiment (i.e., each different gradient strength and direction), a new b-matrix was calculated using analytical expressions we previously derived from Eqs. 2, 3, and 8. $\mathbf{D}_{\text{eff}}$ was then estimated optimally by multivariate weighted linear regression from Eq. 7 (Basser et al., 1992, 1994). These control experiments validated the method of diffusion tensor spectroscopy, i.e., the estimation of an effective diffusion tensor from a series of spin-echo signals. Additionally, the pork loin sample was placed in the bore of the magnet with its grain (i.e., fiber axis) approximately aligned with the x-axis. We previously measured the spin-echo intensity using the protocol described above, and estimated $\mathbf{D}_{\text{eff}} = \mathbf{D}^{0°}$ at 15.0°C. Then we rotated the pork-loin sample by 41° in the x-z plane, repeated the spin-echo experiment, and estimated $\mathbf{D}_{\text{eff}} = \mathbf{D}^{41°}$ at 15.5°C. Here, we construct diffusion ellipsoids from this data.

In other studies, NMR diffusion tensor imaging of *ex vivo* cat brain was performed using the same surface coil and 4.7-Tesla spectroscopy/imaging system described above. Here, a 2D-FT spin-echo, pulsed-gradient sequence, depicted in Fig. 3, was used to acquire diffusion-weighted sagittal images of a cat brain that had been excised 40 h before the experiment. Diffusion gradients were applied along the three orthogonal coordinate directions (read, phase, and slice) in nine noncollinear directions.[3] Collecting a total of 135 images took approximately 5 h. Imaging parameters are given in Table 1.

For each diffusion-weighted image, the echo attenuation is determined in each voxel. The b-matrix is calculated analytically (Mattiello et al., 1993) using Eqs. 7 and 8, including the imaging gradients shown in Fig. 3. Then $\mathbf{D}_{\text{eff}}$ is estimated optimally in each voxel by weighted multivariate linear regression (Basser et al., 1992, 1994).

RESULTS

The estimated $\mathbf{D}_{\text{eff}}$ (cm^2/s) for the pork-loin sample with the grain aligned approximately with the x axis of the magnet $\mathbf{D}^{0°}$ is shown below ± the standard error for each tensor element:

$$\mathbf{D}^{0°} = \left[\begin{pmatrix} 1.0513 & 0.0535 & -0.0040 \\ 0.0535 & 0.9697 & 0.0256 \\ -0.0040 & 0.0256 & 0.8423 \end{pmatrix} + \begin{pmatrix} \pm 0.0055 & \pm 0.0044 & \pm 0.0043 \\ \pm 0.0044 & \pm 0.0053 & \pm 0.0043 \\ \pm 0.0043 & \pm 0.0043 & \pm 0.0051 \end{pmatrix} \right] 10^{-5}. \quad (17)$$

The adjusted coefficient of correlation, $r^2 = 0.999999$; $N = 294$.

The eigenvalues for $\mathbf{D}^{0°}$ are: $\lambda_1 = 1.078 \times 10^{-5}$ (cm^2/s); $\lambda_2 = 0.949 \times 10^{-5}$ (cm^2/s); $\lambda_3 = 0.836 \times 10^{-5}$ (cm^2/s).

An effective diffusion ellipsoid constructed from $\mathbf{D}^{0°}$ using Eq. 12 (Basser et al., 1992, 1994) is shown below in Fig. 4.

[2] For example, we can define new dimensionless scalar invariants, I_1', I_2', and I_3', so that $I_1' = (I_1/3D_w)$; $I_2' = (I_2/3D_w^2)$; $I_3' = (I_3/D_w^3)$.

[3] While nine noncollinear directions were used for convenience, it is sufficient to use only seven noncollinear gradient directions to estimate the six independent elements of the effective diffusion tensor and the scalar, $A(0)$.

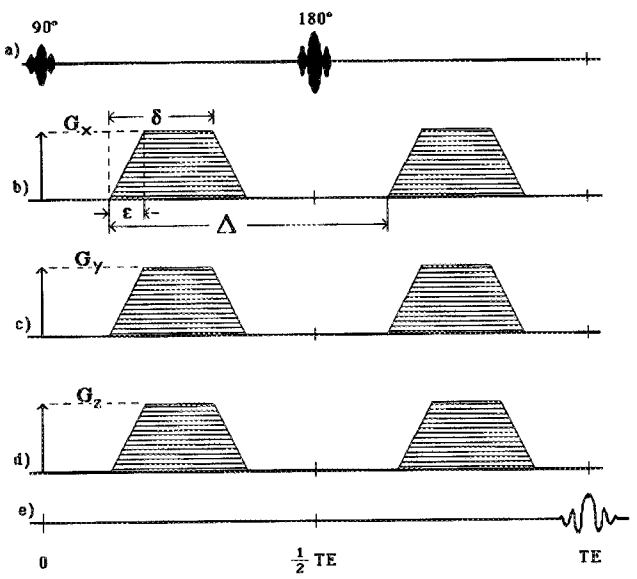

FIGURE 2 RF gradient and pulse sequences used in the pulsed-gradient spin-echo NMR diffusion spectroscopy experiment: (*a*) The 90° and 180° RF pulses in the surface coil. The magnetic field gradients (G/cm) applied in the *x* (*b*), *y* (*c*), and *z* (*d*) directions; (*e*) the received echo signal. *TR* (repetition time) = 15 s; *TE* = 40 ms; δ = 4.2 ms; ε = 0.2 ms; Δ = 22.5 ms. Diffusion gradients must be applied simultaneously when more than one are applied.

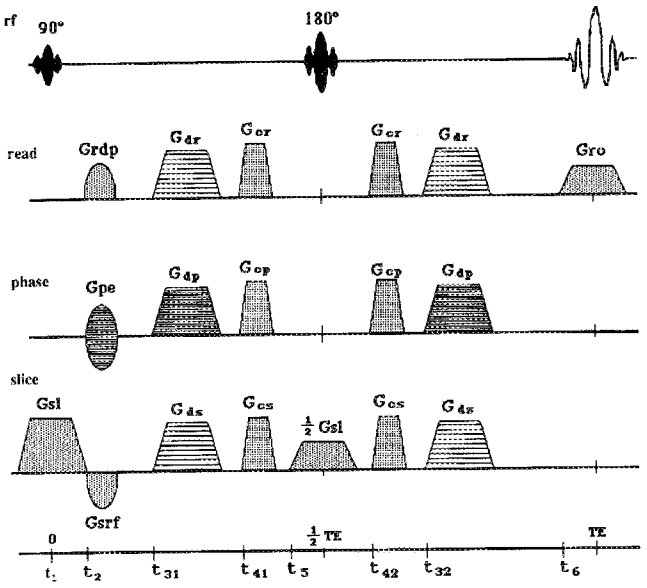

FIGURE 3 The two-dimensional Fourier-transform spin-echo, pulsed-gradient sequence used to acquire NMR diffusion tensor images. The 90° and 180° RF pulses and echo signal are illustrated above. Slice thickness = 5 mm, ε = 0.5 ms, *TE* = 80 ms, the number of phase-encode steps = 128, and the block size = 128. The time at which the gradient pulse turns on during the pulse sequence (t_k), as well as gradient pulse intensities in the read, phase, and slice directions, are shown here and listed in Table 1.

The estimated $\mathbf{D}_{\text{eff}}$ (cm^2/s) for the pork-loin sample with the grain rotated 41° off the *x* axis in the *x*-*z* plane, $\mathbf{D}^{41°}$, is shown below ± the standard error for each tensor element:

$$\mathbf{D}^{41°} = \left[\begin{pmatrix} 0.9761 & 0.0278 & -0.0748 \\ 0.0278 & 0.9529 & -0.0106 \\ -0.0748 & -0.0106 & 0.9653 \end{pmatrix} + \begin{pmatrix} \pm 0.0039 & 0.0031 & \pm 0.0031 \\ \pm 0.0031 & \pm 0.0039 & \pm 0.0031 \\ \pm 0.0031 & \pm 0.0031 & \pm 0.0039 \end{pmatrix} \right] 10^{-5}. \quad (18)$$

The adjusted coefficient of correlation, $r^2 = 0.999999$; $N = 294$.

The eigenvalues for $\mathbf{D}^{41°}$ are: $\lambda_1 = 1.053 \times 10^{-5}$ (cm^2/s); $\lambda_2 = 0.948 \times 10^{-5}$ (cm^2/s); $\lambda_3 = 0.893 \times 10^{-5}$ (cm^2/s).

A diffusion ellipsoid constructed from $\mathbf{D}^{41°}$ using Eq. 12 (Basser et al., 1992, 1994) is shown in Fig. 5, along with its projections on the *x*-, *y*-, and *z*-planes.

Representative estimated effective diffusion tensors for different regions of the cat brain are given below.

Within the ventricle:

$$\mathbf{D}_{\text{eff}} = \begin{pmatrix} 0.2855 & 0.0000 & 0.00711 \\ 0.0000 & 0.2396 & 0.0000 \\ -0.00711 & 0.0000 & 0.2693 \end{pmatrix} \times 10^{-5}(\text{cm}^2/\text{s}); \quad (19)$$

within the cerebellum:

$$\mathbf{D}_{\text{eff}} = \begin{pmatrix} 0.2682 & -0.108 & -0.1366 \\ -0.108 & 0.1491 & -0.0569 \\ -0.1366 & -0.0569 & 0.2699 \end{pmatrix} \times 10^{-5}(\text{cm}^2/\text{s}); \quad (20)$$

and within the corpus callosum:

$$\mathbf{D}_{\text{eff}} = \begin{pmatrix} 0.2747 & 0.045 & 0.0210 \\ 0.045 & 0.0327 & 0.009 \\ 0.0210 & 0.009 & 0.0375 \end{pmatrix} \times 10^{-5}(\text{cm}^2/\text{s}). \quad (21)$$

TABLE 1 Parameters used to calculate the b matrix values for the 4.7 T experiment, derived from a 2D-FT spin-echo pulse sequence for the protocol specified in the Materials and Methods section

i	δ_i	t_i	G_i
	μs	μs	G/mm
1	2450.0	0.0	Gsl + 0.241
			Grdp + 0.214
2	2000.0	1475.0	Gpe + 0.000
			Gsrf + 0.232
			Gd_r 0 to + 1.400
31	4500.0	5525.0	Gd_p 0 to + 1.400
			Gd_s 0 to + 1.400
			Gc_r + 0.500
41	4500.0	15525.0	Gc_p + 0.500
			Gc_s + 0.500
5	2450.0	38525.0	
42		59475.0	
32		69475.0	
6	3714.5	77892.75	Gro + 0.147

The *i*th gradient pulse strengths (G_i), the gradient pulse duration (δ_i), and the time during which the gradient pulses are turned on during the pulse sequences (t_i). The gradient pulses shown in Fig. 3 are defined as G_1 = (Gsl), a 90° slice-selection gradient; G_2 = (Grdp, Gpe, or Gsrf), the read-dephasing, phase-encode, or slice-refocusing gradients, respectively; G_3 = (Gd_r, Gd_p, or Gd_s), the diffusion gradients in the read, phase, and slice directions, respectively; G_4 = (Gc_r, Gc_p, or Gc_s), the crusher gradients in the read, phase, and slice directions, respectively; G_5 = (½Gsl), a 180° slice-gradient; and G_6 = (Gro), the readout gradient.

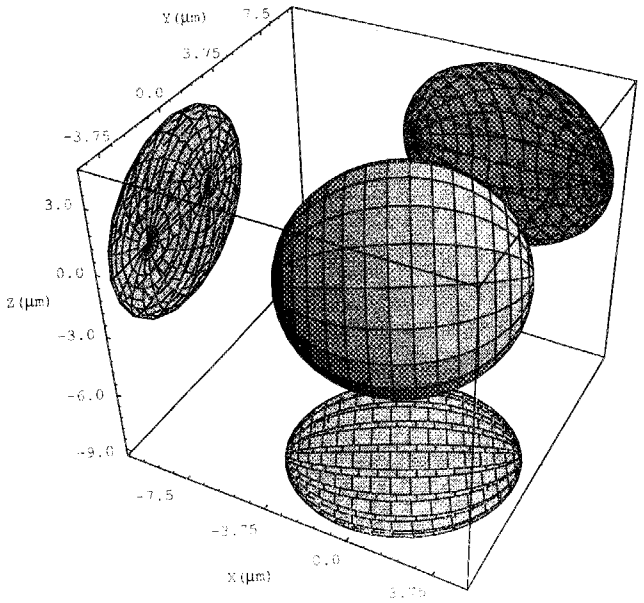

FIGURE 4 Diffusion ellipsoid of a pork loin sample. Its fiber axis is approximately aligned with the x axis of the laboratory frame of reference. Laboratory coordinates X, Y, and Z are displayed in microns. The eigenvector (orthotropic direction) corresponding to the largest eigenvalue (principal diffusivity) defines the polar axis of the ellipsoid.

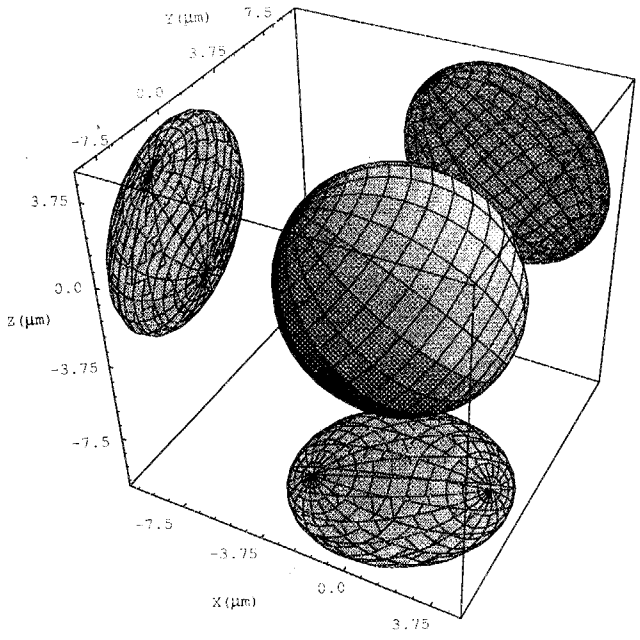

FIGURE 5 Diffusion ellipsoid for the same pork loin sample shown in Fig. 4, now rotated by 41° in the x-z plane.

Fig. 6 shows a T_1-weighted image of a sagittal slice of an excised cat brain. Using the method described above, we estimated an effective diffusion tensor in each voxel within a 16 × 16-pixel region of interest (shown by the *inset* in Fig. 6), which contains a portion of the corpus callosum and a ventricle. Fig. 7 shows this 16 × 16-pixel ROI as a gray scale image. Juxtaposed is an image of the corresponding effective

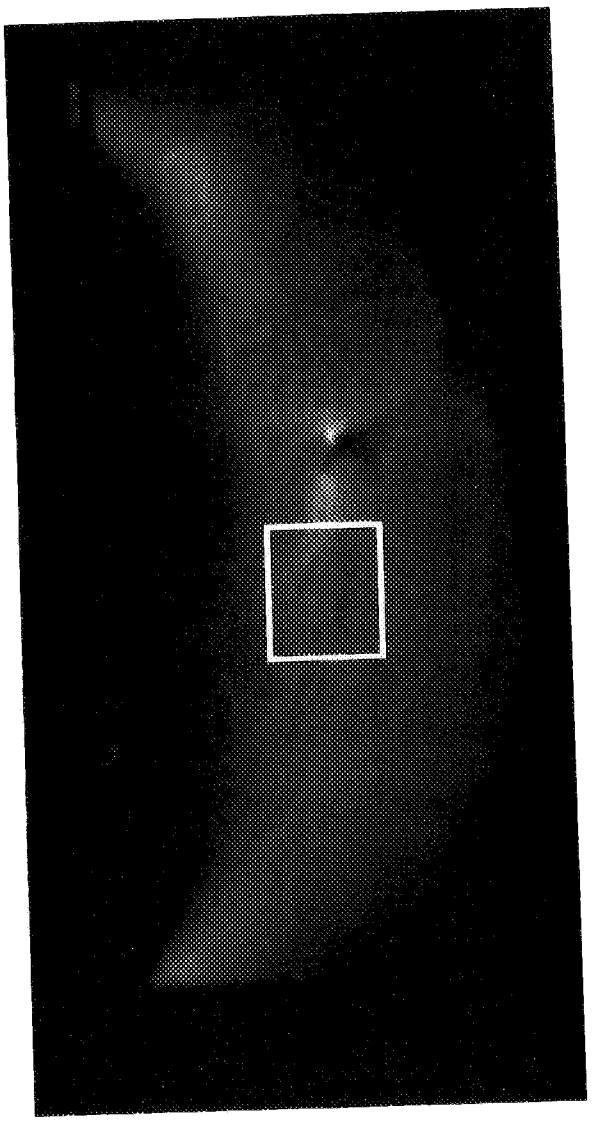

FIGURE 6 A T_1-weighted image of a sagittal section of an excised cat brain with the cerebellum at the top of the page. The box encloses a 16 × 16-pixel region of interest, containing a portion of the corpus callosum and a ventricle filled with CSF.

diffusion ellipsoids that were constructed from $\mathbf{D}_{\text{eff}}$ estimated in each of the 16 × 16 corresponding voxels. Fig. 8 shows an image of the first scalar invariant, $\text{Tr}(\mathbf{D}_{\text{eff}})$, for the same sagittal slice of excised cat brain. Again, the ROI is shown by the inset in Fig. 8.

DISCUSSION

While these diffusion spectroscopy data have been published elsewhere (Basser et al., 1994), we refer to them here to illustrate that they can be used to construct diffusion ellipsoids whose polar axes (which represent the fiber axes) follow the mechanical rotation of the tissue sample, as demonstrated by the tipping of the polar axis of the diffusion ellipsoid by 41° from that shown in Fig. 4 to that shown in Fig. 5. Both effective diffusion ellipsoids shown in Figs. 4 and 5 are only slightly prolate, presumably because the diffusion time defined as $\Delta - \delta/3 = 22.5$ ms corresponds to a

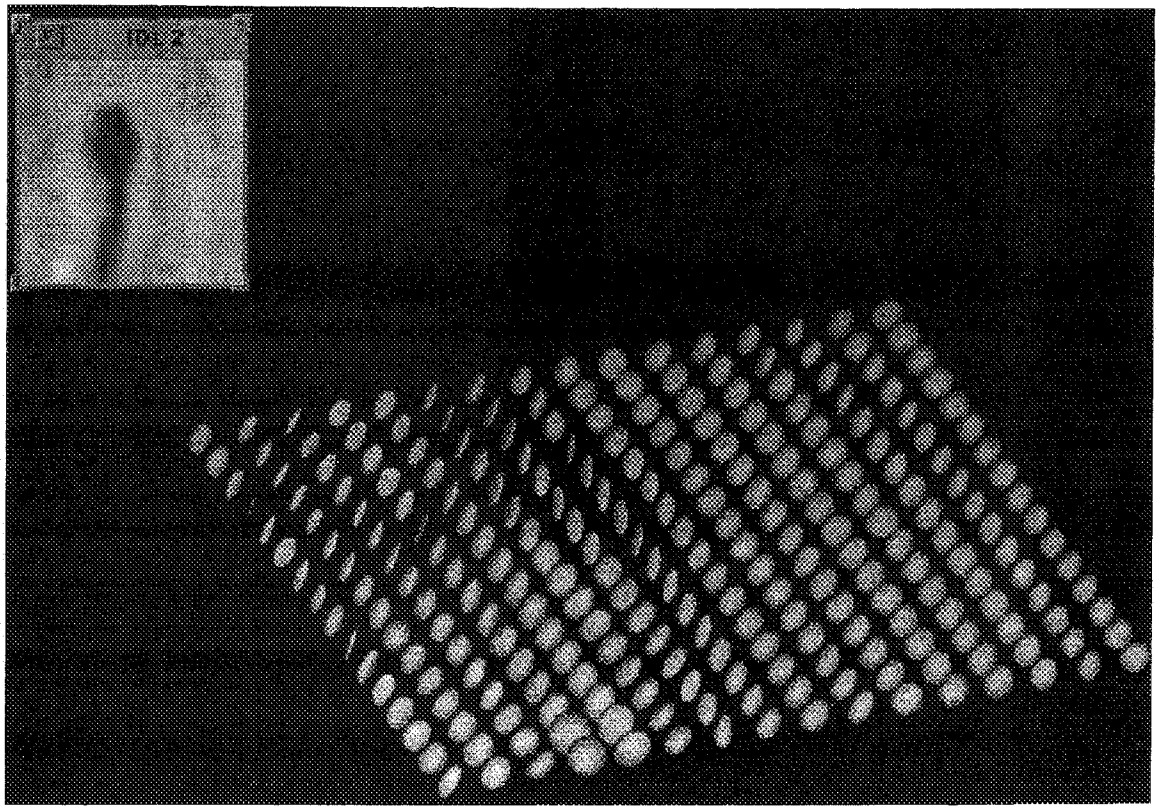

FIGURE 7 Effective diffusion ellipsoid image of the ROI shown in Fig. 6. The 16 × 16 array of ellipsoids is displayed above a gray scale image of the first scalar invariant of the effective diffusion tensor, $\mathrm{Tr}(\mathbf{D}_{\mathrm{eff}})$.

mean diffusion distance of only 4.7 μm, which may be too short for the majority of spin-labeled protons to encounter diffusion barriers. In addition, the store-bought meat sample represents a worst-case test of this method, since its membranes and other anisotropic structures may have disintegrated during the freezing and aging process.

While individual components of $\mathbf{D}_{\mathrm{eff}}$ for pork loin (in Eq. 17 and 18) differ by hundreds of percentage points, the eigenvalues and scalar invariants of $\mathbf{D}_{\mathrm{eff}}$ differ by no more than one percentage point. This is what we would expect, since these invariant quantities reflect intrinsic properties of the medium, such as the mean water mobility, that may reflect changes in the sample's microstructure but should not be affected by its orientation within the magnet. We anticipate that these scalar invariants (or functions of them) will be useful in NMR imaging of anisotropic tissues.

The effective diffusion ellipsoids constructed for each of the 16 × 16 voxels shown in Fig. 7 correspond to the known tissue composition and fiber orientation in this region of brain tissue. For example, the fibers within the corpus callosum are properly oriented (i.e., they correlate with known anatomy), while a ventricle filled with CSF is depicted by a large spherical ellipsoid, indicating isotropic diffusion. Gray and white matter are also easily distinguishable. Moreover, spatial gradients in fiber-tract orientation on a multivoxel length scale are also seen.

In Fig. 8, the image of the trace of the effective diffusion tensor, $I_1 = \mathrm{Tr}(\mathbf{D}_{\mathrm{eff}})$, provides information not contained in the T_1-weighted image shown in Fig. 6. For example, in Fig. 8 it is easy to distinguish regions of CSF, gray and white matter, fissures, and the corpus callosum, none of which were apparent in the proton image of the same tissue. While these differences may be apparent in T_1 or T_2 weighted images, the scalar invariants may provide additional information with which to segment tissue types.

Using two-dimensional Fourier-transform spin-echo, pulsed-gradient imaging sequences, the acquisition of enough diffusion-weighted images to estimate a diffusion tensor in each voxel accurately is prohibitively long (for many in vivo biomedical applications). However, Eqs. 7 and 8, and the methods presented above to estimate and display the effective diffusion tensor, apply equally well to rapid imaging techniques such as echo-planar imaging (Turner and LeBihan, 1990; Turner et al., 1990), with which it is possible to acquire diffusion-weighted images in a fraction of the time. In principle, the sequences needed to estimate an effective diffusion tensor can be incorporated into virtually any imaging sequence. In a subsequent paper, we will show that diffusion tensor imaging can be performed on in vivo human brain without motion artifacts in about 20 min (Basser et al., 1993).

CONCLUSION

In T_1, T_2, and (apparent) diffusion MRI, one estimates these scalar parameters that specify the chemical or physical state

FIGURE 8 Image of $Tr(\mathbf{D}_{eff})$, calculated for the sagittal section of excised cat brain shown in Fig. 6. The box indicates the ROI from which the diffusion ellipsoids were constructed in Fig. 7.

of tissue within a voxel. To glean information about their spatial distribution, one must make *intervoxel* comparisons. In contrast, in diffusion *tensor* MRI we estimate a tensor, $\mathbf{D}_{eff}$, that inherently contains *intravoxel* structural and dynamic information, embodied in the shape of the effective diffusion ellipsoid and contained in the scalar invariants. Specifically, the eigenvectors of $\mathbf{D}_{eff}$ can be used to construct a local frame of reference within a voxel (which we associate with the local orthotropic directions of the medium); and the eigenvector of the largest eigenvalue defines the local fiber-tract axis. The eigenvalues of $\mathbf{D}_{eff}$ are the diffusion coefficients in these orthotropic directions. The effective diffusion ellipsoid displays the mean diffusion distances in each of the three principal directions during the diffusion time, defined by the gradient pulse sequence. The three scalar invariants of $\mathbf{D}_{eff}$ contain additional information that is independent of fiber orientation per se, which we anticipate will reflect subtle changes in the microstructure of the medium, and which are readily measured and monitored.

Characterizing diffusive motions of protons and other metabolites within a single voxel of an anisotropic medium may have great potential biological significance. For example, in ontogeny, it would provide a means of monitoring the development of anisotropic tissues and ordered structures in vivo, both noninvasively and nondestructively. In physiology, it would provide a means of measuring diffusivities of water and metabolites parallel to and perpendicular to fiber tract directions, and would even permit one to infer cell membrane, intracellular, and interstitial diffusivities from an appropriate microstructural model of the tissue. In anatomy, it would provide a means of producing fiber-tract orientation maps, of classifying (segmenting) different tissue types, and even of visualizing muscle and nerve fiber tracts individually. In pathology, it may provide a means of diagnosing and monitoring the progression of various disease states, such as diffuse demyelination, ischemia (including stroke), and edema (even helping to distinguish between cytotoxic, vasogenic, and interstitial edemas). Finally, one could imagine using this technique to test nonmagnetic samples nondestructively (e.g., gels, and in vitro cell and tissue cultures).

As a final note, the effective hydraulic, electrical, and thermal conductivity tensors (DeGroot and Mazur, 1984) that relate gradients in hydrostatic pressure, electrical potential, and temperature to solvent, electrical current, and heat fluxes, respectively (Onsager, 1931; Onsager, 1931) should share the same orthotropic directions (eigenvectors) as the effective diffusion tensor, used above to construct fiber-tract direction maps, although obviously they will have different eigenvalues.

This work was performed at the National Institutes of Health In Vivo NMR Center. We thank Alan Olson for his technical support; Robert Turner, Philippe Douek, and Brad Roth for their thoughtful comments; and Barry Bowman for his meticulous editing of the manuscript.

REFERENCES

Basser, P. J., and D. LeBihan, 1992. Fiber orientation mapping in an anisotropic medium with NMR diffusion spectroscopy. *Proc. 11th Annu. Meet. SMRM, Berlin.* 1:1221.

Basser, P. J., D. LeBihan, and J. Mattiello. 1994. The effective self-diffusion tensor: its relationship to and estimation from the NMR spin-echo. *J. Magn. Res. Ser.B.* In press.

Basser, P. J., J. Mattiello, and D. LeBihan. 1992. Diagonal and off-diagonal components of the self-diffusion tensor: their relation to and estimation from the NMR spin-echo signal. *Proc. 11th Annu. Meet. SMRM, Berlin.* 1:1222.

Basser, P. J., J. Mattiello, R. Turner, and D. LeBihan. 1993., Diffusion tensor echo-planar imaging of human brain. *Proc. 12th Annu. Meet. SMRM, New York.* 1404.

Bloch, F. 1946. Nuclear induction. *Phys. Rev.* 70:460–474.

Chenevert, T. L., J. A. Brunberg, and J. G. Pipe. 1990. Anisotropic diffusion in human white matter: demonstration with MR techniques in vivo. *Radiology.* 177:401–405.

Cleveland, G. G., D. C. Chang, and C. F. Hazlewood. 1976. Nuclear magnetic resonance measurement of skeletal muscle. Anisotropy of the diffusion coefficient of the intracellular water. *Biophys. J.* 16:1043–1053.

Cory, D. G. 1990. Measurement of translational displacement probabilities

by NMR: an indicator of compartmentation. *Magn. Reson. Med.* 14: 435–444.

DeGroot, S. R., and P. Mazur. 1984. Non-equilibrium thermodynamics. Dover Publications. 510 pp.

Doran, M., J. V. Hajnal, N. Van Bruggen, M. D. King, I. R. Young, and G. M. Bydder. 1990. Normal and abnormal white matter tracts shown by MR imaging using directional diffusion weighted sequences. *J. Comput. Assist. Tomogr.* 14:865–873.

Douek, P., R. Turner, J. Pekar, N. Patronas, and D. LeBihan. 1991. MR color mapping of myelin fiber orientation. *J. Comput. Assist. Tomogr.* 15:923–929.

Fullerton, G. D., I. L. Cameron, and V. A. Ord. 1985. Orientation of tendons in the magnetic field and its effect on T2 relaxation times. *Radiology.* 155:433–435.

Fung, Y. C.. 1977. A first course in continuum mechanics. Prentice-Hall, Inc. 344 pp.

LeBihan,, D. 1991. Molecular diffusion nuclear magnetic resonance imaging. *Magn. Reson. Q.* 7:1–30.

LeBihan, D., and E. Breton. 1985. Imagerie de diffusion in-vivo par resonance magnetique nucleaire. *Cr. Acad. Sci. (Paris).* 301: 1109–1112.

LeBihan, D., E. Breton, D. Lallemand, P. Grenier, E. Cabanis, and M. Laval-Jeantet. 1986. MR imaging of intravoxel incoherent motions: application to diffusion and perfusion in neurologic disorders. *Radiology.* 161:401–407.

LeBihan, D., R. Turner, and P. Douek. 1993. Is water diffusion restricted in human brain white matter? An echo-planar NMR imaging study. *NeuroReport.* 4:887–890.

Mattiello, J., P. J. Basser, and D. LeBihan. 1994. An analytical expression for the b-matrix in NMR diffusion tensor imaging and spectroscopy. *J. Magn. Reson.* In press.

Merboldt, K. D., W. Hanicke, and J. Frahm. 1985. Self-diffusion NMR imaging using stimulated echoes. *J. Magn. Reson.* 64:479–486.

Moseley, M. E., Y. Cohen, J. Kucharczyk, J. Mintorovitch, H. S. Asgari, M. R. Wendland, J. Tsuruda, and D. Norman. 1990. Diffusion-weighted MR imaging of anisotropic water diffusion in cat central nervous system. *Radiology.* 176:439–446.

Neeman, M., J. P. Freyer, and L. O. Sillerud. 1990. Pulsed-gradient spin-echo studies in NMR imaging. Effects of the imaging gradients on the determination of diffusion coefficients. *J. Magn. Reson.* 90: 303–312.

Onsager, L. 1931. Reciprocal relations in irreversible processes. Part I. *Phys. Rev.* 37:405.

Onsager, L. 1931. Reciprocal relations in irreversible processes. Part II. *Phys. Rev.* 38:2265.

Stejskal, E. O. 1965. Use of spin echoes in a pulsed magnetic-field gradient to study restricted diffusion and flow. *J. Chem. Phys.* 43:3597–3603.

Stejskal, E. O., and J. E. Tanner. 1965. Spin diffusion measurements: spin echoes in the presence of time-dependent field gradient. *J. Chem. Phys.* 42:288–292.

Tanner, J. E. 1978. Transient diffusion in system partitioned by permeable barriers. Application to NMR measurements with a pulsed field gradient. *J. Chem. Phys.* 69:1748–1754.

Torrey, H. C. 1956. Bloch equations with diffusion terms. *Phys. Rev.* 104: 563–565.

Turner, R., and D. LeBihan. 1990. Single shot diffusion imaging at 2.0 Tesla. *J. Magn. Reson.* 86:445–452.

Turner, R., D. LeBihan, J. Maier, R. Vavrek, L. K. Hedges, and J. Pekar. 1990. Echo-planar imaging of intravoxel incoherent motion. *Radiology.* 177:407–414.